Journal of Alloys and Compounds 523 (2012) 66–71

Contents lists available at SciVerse ScienceDirect

Journal of Alloys and Compounds

journal homepage: www.elsevier.com/locate/jallcom

Effect of sintering temperature on structural, magnetic properties of lithium chromium ferrite

R.P. Patil[a,*], P.P. Hankare[a,*], K.M. Garadkar[a], R. Sasikala[b]

[a] Department of Chemistry, Shivaji University, Kolhapur 416004, India
[b] Chemistry Division, Bhabha Atomic Research Center, Mumbai 400085, India

ARTICLE INFO

Article history:
Received 27 October 2010
Received in revised form
24 December 2011
Accepted 4 January 2012
Available online 12 January 2012

Keywords:
Ferrites
Sol–gel synthesis
X-ray diffraction
Raman spectra
TEM

ABSTRACT

Nanocrystalline mixed lithium–chromium ferrites were prepared by using sol–gel method. The samples were sintered at different temperatures in air. Their structural and magnetic properties were studied by X-ray diffraction, scanning electron microscopy, transmission electron microscopy, Raman scattering, FT-IR and magnetic hysteresis loop tracer techniques. The X-ray diffraction patterns reveal that all the samples consist of nanocrystalline single cubic phase structure. The morphological studies of synthesized nanocrystalline samples were obtained from the scanning electron microscopy and transmission electron microscopy techniques. Raman scattering and FT-IR studies indicate that the spinel phase formation takes place at higher sintering temperature. The magnetic studies show that, the ferrimagnetic behavior increases with sintering temperature.

1. Introduction

Ferrites are magnetic semiconductors which cannot be replaced by any other magnetic material, because of their stable, relatively inexpensive, ease formation. These materials have interesting structural, electrical and magnetic properties, which make them in widespread applications such as electronics and telecommunication industries [1]. These properties are tunable with chemical composition, method of preparation, sintering temperature, sintering time, etc. [2].

Among various ferrites, lithium and metal substituted lithium ferrites have been attractive structural and magnetic features that render them as a potential material for various technological applications such as, lithium batteries, recording heads, transformer cores, and noise filters [3–11]. The structural and magnetic properties of these ferrite systems with respect to different sintering temperature conditions have been reported by many workers [12,13]. In this communication, we report the effects on structural and magnetic properties of the $Li_{0.5}Fe_{1.5}Cr_{1.0}O_4$ samples with sintering temperature (T_S) from 673 to 973 K.

2. Experimental details

Analytical grade chromium nitrate [$Cr(NO_3)_3{\cdot}9H_2O$], iron nitrate [$Fe((NO_3)_2{\cdot}9H_2O$], lithium nitrate [$LiNO_3$] and citric acid [$C_6H_8O_7{\cdot}H_2O$] were used to prepare $Li_{0.5}Fe_{1.5}Cr_{1.0}O_4$ by a sol–gel method. Metal nitrates and citric acid were dissolved in deionized water with 1:1 molar ratio. The pH of the solution was adjusted to 9.0–9.5 using ammonia solution. Then, the solution was heated at 353 K, which results gel formation. When ignited, the dried gel burnt in a self propagating combustion manner until it was converted into a floppy loose powder. This powder was then sintered at different temperatures such as, 673, 773, 873 and 973 K for 8 h. The sintered powders were granulated and using 2% polyvinyl alcohol as a binder were uniaxially pressed at a pressure of 8 ton/cm^2 to form pellet specimens.

The structural studies of the sintered samples were obtained by X-ray diffraction technique using a Philips PW-1710 X-ray diffractometer with Cu Kα radiation (λ = 1.54056 Å). Raman spectra and FT-IR studies were used for interpretation of the vibrational modes in mixed metal oxides. Microstructural analyses of the samples were carried out using transmission electron microscope (TEM-Model Philips 200 CX) operating at a voltage of 120 kV and also using scanning electron microscope (JEOL-JSM 6360 Microscope). The high field hysteresis loop tracer (Magenta) was used to measure the saturation magnetization, coercivity and remanance magnetization of all the samples as function of sintering temperature.

3. Results and discussion

3.1. X-ray diffraction studies

X-ray powder diffraction pattern of the $Li_{0.5}Fe_{1.5}Cr_{1.0}O_4$ samples as prepared and sintered at different temperatures are shown in Fig. 1. X-ray diffraction data shows that, the cubic phase is observed at 973 K. The diffraction pattern of as prepared sample

* Corresponding authors. Tel.: +91 231 2609381.
E-mail addresses: raj_rbm_raj@yahoo.com (R.P. Patil), p_hankarep@rediffmail.com (P.P. Hankare).

0925-8388/$ – see front matter © 2012 Elsevier B.V. All rights reserved.
doi:10.1016/j.jallcom.2012.01.025

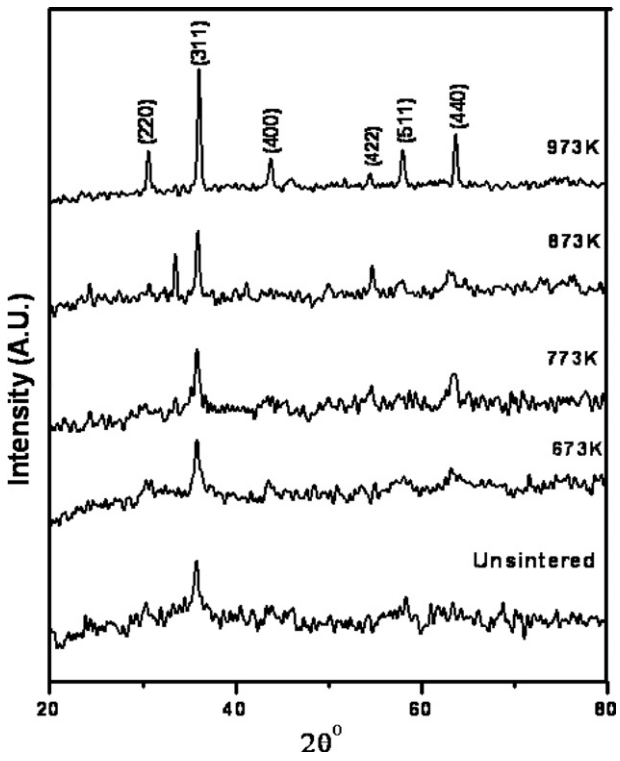

Fig. 1. X-ray diffraction patterns of $Li_{0.5}Fe_{1.5}Cr_{1.0}O_4$ sintered at different temperatures.

confirms the amorphous in nature; while the remaining samples are in crystalline in nature. On increasing the sintering temperature, the diffraction peaks become narrowing and sharper, suggesting the increase in particle size and crystallinity of the samples. The particle size was calculated from most intense peak (3 1 1) using Scheerer formula. It is observed that the particle size increases with the sintering temperature as shown in Fig. 2. This overall data reveals the formation of nanocrystalline nature of all sintered samples. The crystalline size with lattice constants of the samples are summarized in Table 1. The sharp diffraction peaks are an indication of the high surface and bulk mobility in solid phase, due to the higher orientation of atom in the crystal structure, which is similar to the results reported by Trentler et al. [14]. The enhancement of

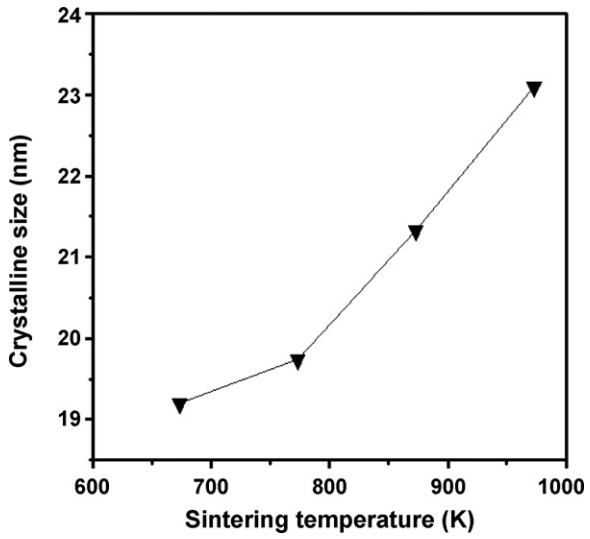

Fig. 2. Plot of crystalline size (nm) vs temperature in K.

Table 1
Data for lattice parameter and crystalline size of the composition $Li_{0.5}Fe_{1.5}Cr_{1.0}O_4$ with sintering temperature.

Temperature (K)	Lattice parameter (Å)	Crystalline size (nm)
Unsintered	7.44	18.33
673	8.16	19.20
773	8.26	19.74
873	8.27	21.33
973	8.31	23.10

the crystalline nature of the sintered samples is attributed that the decrease of the crystalline volume ratio of the samples, and hence due to the size enlargement of the nuclei [15].

3.2. Electron microscopy

Fig. 3a represents the typical transmission electron micrograph of the $Li_{0.5}Fe_{1.5}Cr_{1.0}O_4$ ferrite sintered at 973 K for 8 h. It reveals the narrow size distribution of nanocubes with an almost uniform shape and particles are around 50–100 nm size can be clearly seen in the micrograph. These particles consist of a large number of small particles held together by interfacial forces which are responsible for the spherical shape of larger agglomerate particles. Appearance of agglomeration has also been reported by Sonal Singhal et al. [16]. Selected area electron diffraction (SAED) pattern of the particle is

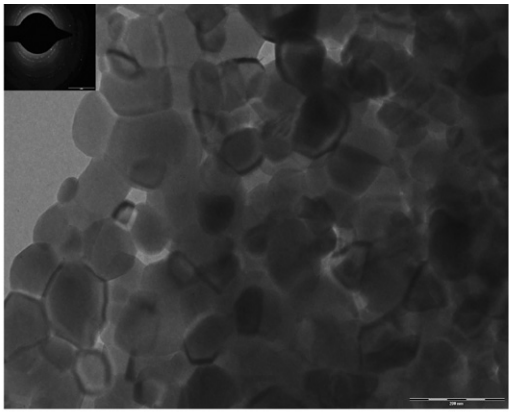

(a) TEM images of $Li_{0.5}Fe_{1.5}Cr_{1.0}O_4$ sintered at 973 K

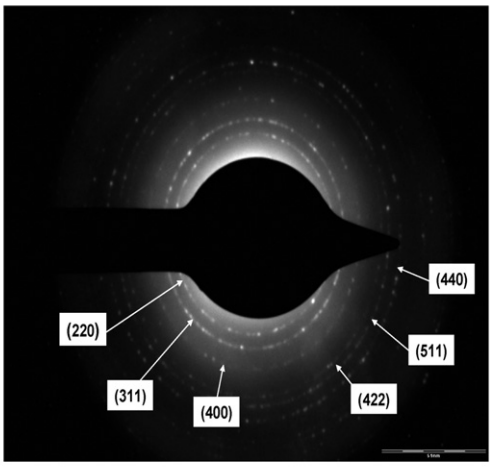

(b) SAED pattern of $Li_{0.5}Fe_{1.5}Cr_{1.0}O_4$ sintered at 973 K

Fig. 3. (a) TEM images of $Li_{0.5}Fe_{1.5}Cr_{1.0}O_4$ sintered at 973 K and (b) SAED pattern of $Li_{0.5}Fe_{1.5}Cr_{1.0}O_4$ sintered at 973 K.

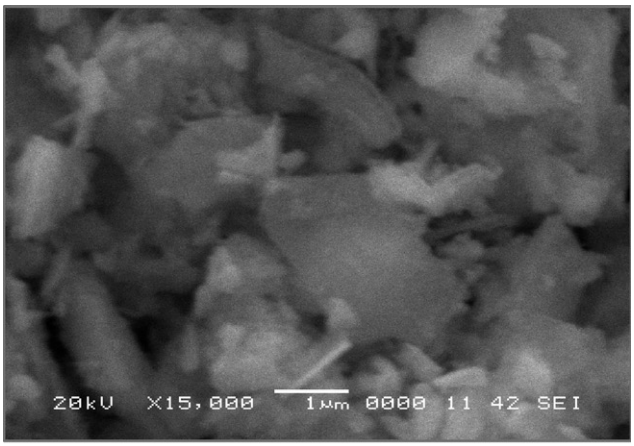

a) Unsintered

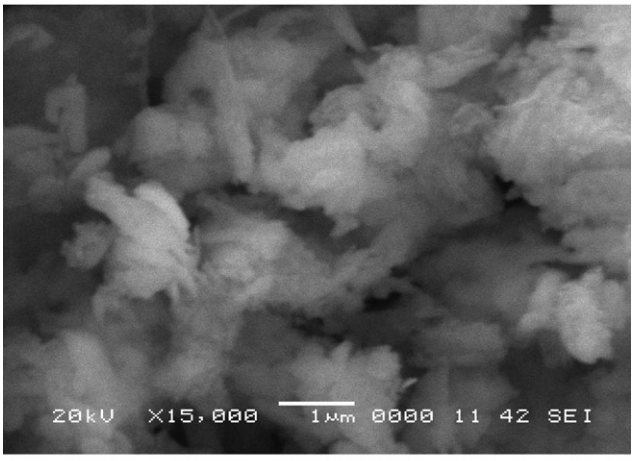

b) 873K

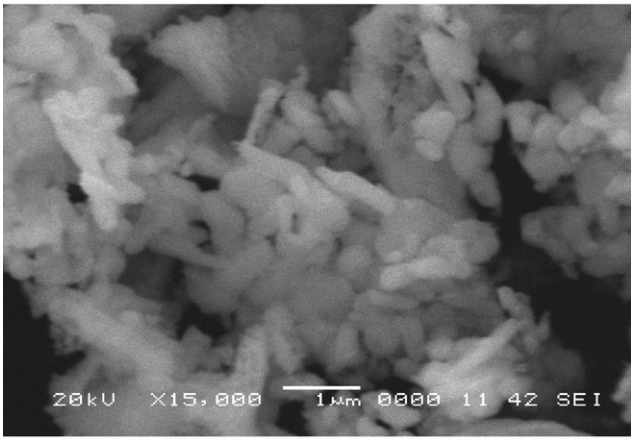

c) 973 K

Fig. 4. SEM images of $Li_{0.5}Fe_{1.5}Cr_{1.0}O_4$ sintered at: (a) unsintered, (b) 873 K and (c) 973 K.

shown in Fig. 3b and also suggests the nanocrystalline nature of the sample.

The morphological features were also studied using SEM technique. The microstructures of the samples are seen; which absolutely tuned with sintering temperature and doping of chromium concentration. The typical scanning electron micrographs of sample and samples sintered at 873 and 973 K are shown in Fig. 4a–c. It was seen that, the grain size and crystallinity is increased significantly with increasing the sintering temperature and moreover the particle size becomes more uniform at higher sintering temperatures. At the sintering temperature of 973 K, substantial grain growth occurs in which the ferrite grain is well crystalline in nature.

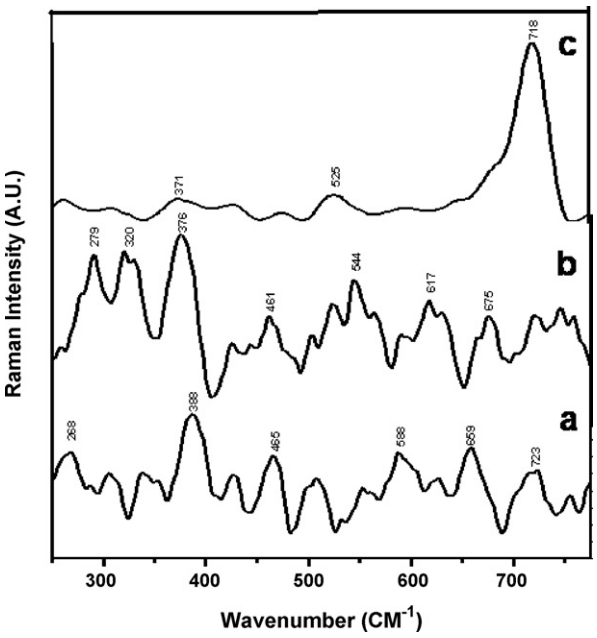

Fig. 5. Effect of sintering temperature on Raman scattering spectra of $Li_{0.5}Fe_{1.5}Cr_{1.0}O_4$: (a) unsintered, (b) 773 K and (c) 973 K.

3.3. Raman studies

Raman scattering spectra have been investigated to evaluate the local structure of lithiated oxides used as electrode materials for lithium-ion batteries [17–19]. Fig. 5a–c shows the typical Raman

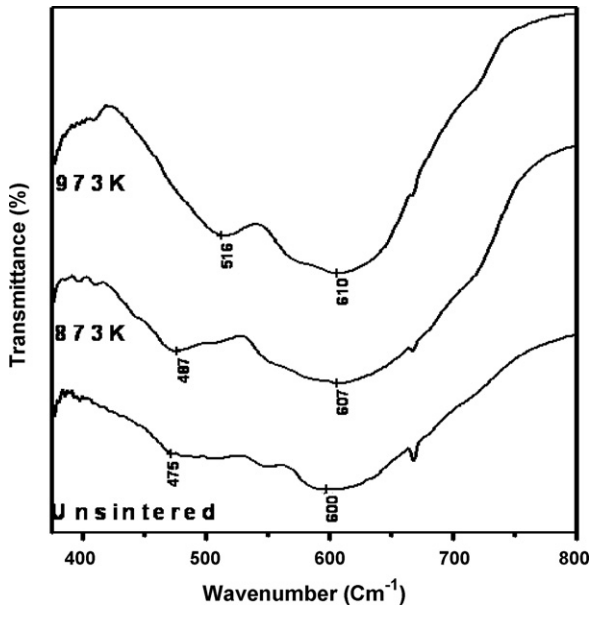

Fig. 6. Effect of sintering temperature on IR spectrum of $Li_{0.5}Fe_{1.5}Cr_{1.0}O_4$: (a) unsintered, (b) 873 K and (c) 973 K.

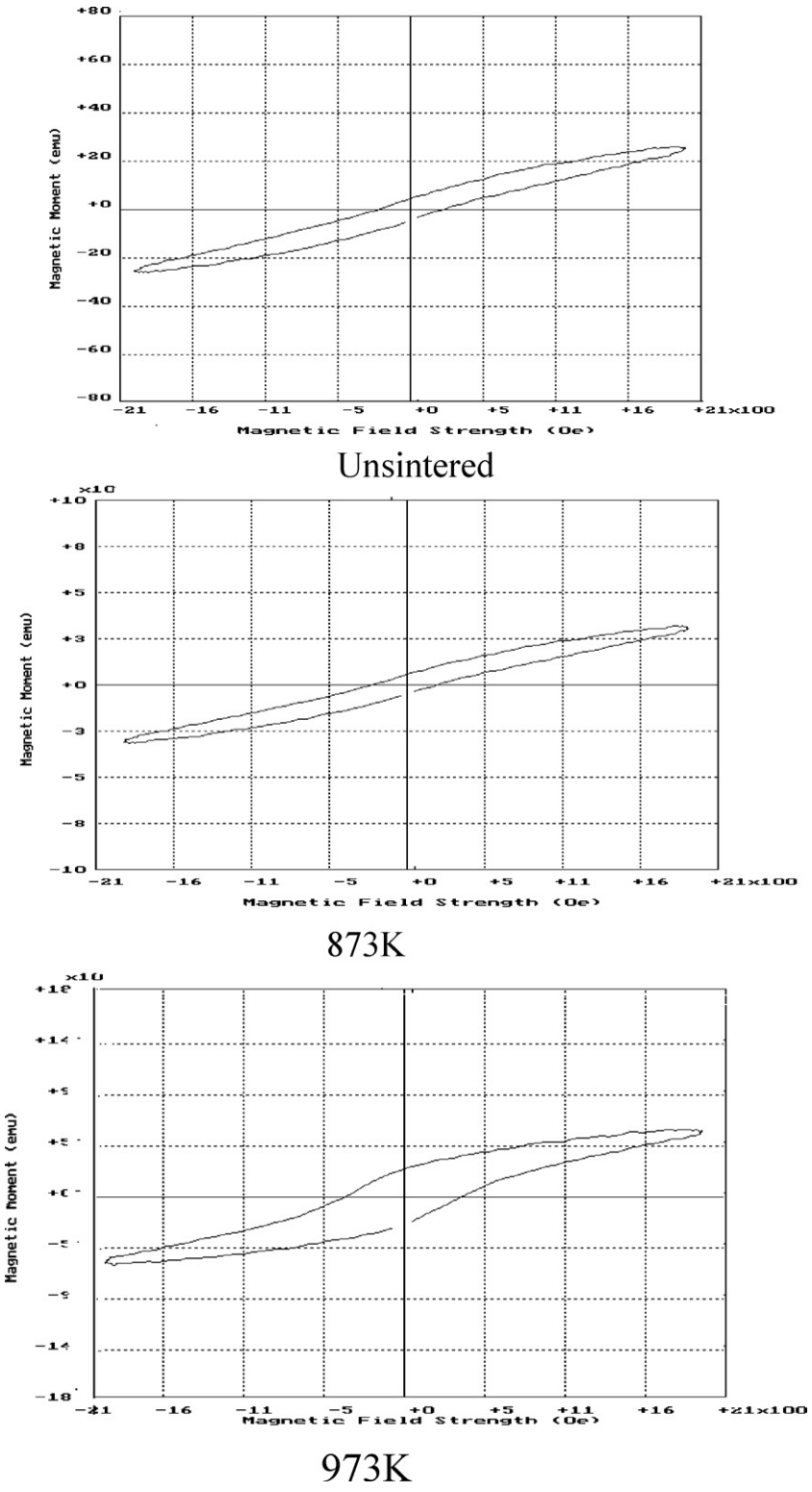

Fig. 7. Magnetic hystersis loop for $Li_{0.5}Fe_{1.5}Cr_{1.0}O_4$ sintered at different temperatures: (a) unsintered, (b) 873 K and (c) 973 K.

Table 2
Data for coercivity (H_c), Saturation magnetization (M_s), remanence magnetization (M_r) and magnetic moment of the composition $Li_{0.5}Fe_{1.5}Cr_{1.0}O_4$ with sintering temperature.

Temperature (K)	Coercivity (H_c)	Saturation magnetization (M_s) emu/g	Remanence magnetization (M_r) emu/g	$R = \frac{M_r}{M_s}$	Magnetic moment (B.M.)
Unsintered	196.43	26.45	4.90	0.18	0.9625
673	227.27	27.45	8.36	0.30	0.9988
773	324.68	28.41	7.89	0.27	1.033
873	330.10	32.40	5.61	0.17	1.179
973	349.03	59.61	20.29	0.34	2.169

spectra of the unsintered and sintered $Li_{0.5}Fe_{1.5}Cr_{1.0}O_4$ spinel in the spectral region 200–800 cm^{-1}. A common feature of these spectra is the presence of strong band around 750 cm^{-1} and a group of bands in the range of 200–500 cm^{-1} with weaker intensity. Raman spectra can solve the problem of phase determination when various environments are present. The effect of sintering on Raman scattering (RS) spectral data shows that the cubic crystalline phase is observed in the sample sintered at 973 K. In these samples, the ordered spinel phase is observed; the narrow peak is due to the presence of Cr_2O_3. The broad band near 718 cm^{-1} is assigned to a Cr—O stretching vibration of mixed chromium–iron oxide and two bands having weak intensity are observed at 371 and 525 cm^{-1}. The RS peaks at lower value 371 and 525 cm^{-1} have assigned the E_g symmetry whereas the peak located at 718 cm^{-1} is the F_{2g} symmetry. It is speculated that the intensity of the Raman spectrum at 525 cm^{-1} is closely related to the chromium average oxidation state in spinel phase. The sharp peak observed with increase in sintering temperature indicates the formation of single crystalline phase structure in spinel ferrites.

3.4. FT-IR studies

Fig. 6 shows the FT-IR spectra of $Li_{0.5}Fe_{1.5}Cr_{1.0}O_4$ spinel in the spectral region 200–800 cm^{-1} unsintered and sintered (at 873 and 973 K) samples. The spectra have been used to locate the band positions. The higher frequency band is observed at around 600 cm^{-1} (ν_1) and lower frequency at around 500 cm^{-1} (ν_2). The absorption bands observed within this range is an indication of the formation of single phase spinel structure [20]. Bands ν_1 and ν_2 are assigned to the intrinsic vibration of tetrahedral and octahedral complexes [21]. The intensity of these bands appears to increases with increasing sintering temperature. The difference in band positions is attributed to the difference in the Fe^{3+}–O^{2-} and Cr^{3+}–O^{2-} distances for tetrahedral and octahedral sites due to temperature effect. It has been observed in the present composition, the band positions ν_1 and ν_2 changes slightly due to the effect sintering temperature on distribution of Cr^{3+} and Fe^{3+} ions at octahedral and tetrahedral sites.

3.5. Magnetic measurements

The hysteresis studies of system, $Li_{0.5}Fe_{1.5}Cr_{1.0}O_4$ was carried out using a magenta B-H loop tracer. The hysteresis loops are shown in Fig. 7a–c. The ferrimagnetic behavior was shown by all the samples with increasing sintering temperature. The variation in saturation magnetization (M_s), remanance magnetization (M_r) and coercivity (H_c) as a function of temperature is depicted in Table 2. The M_s values measured for the samples gradually increased with the sintering temperature. The lower M_s values associated to the particles with smaller size, which could be attributed to two factors. First, surface distortion due to interaction of transition metal ions with the oxygen atoms in the spinel lattice can reduce the net magnetic moment in the particle [22]. Second, the magneto crystalline anisotropy of the particles is depending on the degree of crystallity of the nanoparticles and this will cause a significant reduction of magnetic moment within the particles, as a result of the magnetocrystalline anisotropy distortion. From the hystersis loop, the ratio, R of the remanance to the saturation magnetization (M_r/M_s) is derived to determine whether the intergrain exchanges exist [23]. Stoner and Wohlfarth have reported $R = 0.5$ for randomly oriented non-interacting particles, while for $R < 0.5$, the particles interact by magnetostatic interactions [24] and the exchange-coupled interaction exists when $R > 0.5$. In this study, for all compositions, R values are seen to be less than 0.5 indicating that the particles interact by magnetostatic interactions. The experimental magnetic moment n_β in BM as calculated by following relation [25].

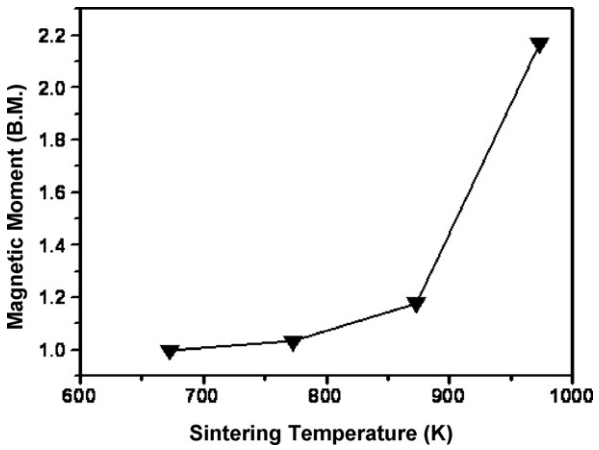

Fig. 8. Effect of sintering temperature on magnetic moment of $Li_{0.5}Fe_{1.5}Cr_{1.0}O_4$ composition.

$$n_\beta = \frac{MW \times M_s}{5585}$$

where MW is the molecular weight of composition (in g); M_s is the saturation magnetization (in Oe); 5585, magnetic factor.

The magnetic moment data (Fig. 8 and Table 2) clearly indicate that, as the sintering temperature increases the magnetic moment increases.

4. Conclusion

Nanocrystalline chromium substituted lithium ferrite was synthesized by the sol–gel method. The ferrite was sintered at different temperatures to study the effect of sintering on its various properties. X-ray diffraction patterns reveal the broadening of major peaks and are indication of spinel phase formation. The effect of the sintering temperature on its grain morphology and microstructure of the samples is studied using SEM and TEM method. The Raman and FT-IR studies indicate that, the spinel phase formation occurs at higher sintering temperature. The magnetic study, for all compositions, R values are seen to be less than 0.5 indicating that the particles interact by magnetostatic interactions and also indicate that, as the sintering temperature increases the magnetic moment increases.

Acknowledgement

The authors are thankful to DAE-BRNS, Mumbai for financial assistance through Major Research Project No. 2009/37/41/BRNS/2231.

References

[1] J.B. Goodenough, Magnetism and Chemical Bond, New York, Wiley, 1966.
[2] G. Rangamohan, D. Ravinder, A.V. RamanaReddy, B.S. Bayanor, Mater. Lett. 40 (1999) 39.
[3] G.O. White, C.E. Patton, J. Magn. Magn. Mater. 9 (1978) 299.
[4] R.K. Puri, V. Varshney, J. Phys. Chem. Solids 44 (1983) 655.
[5] R.G. Kharabe, S.A. Jadhav, A.M. Shaikh, D.R. Patil, B.K. Chougale, Mater. Chem. Phys. 72 (2001) 77.
[6] R. Laishram, S. Phanjoubam, H.N.K. Sharma, C. Prakash, J. Phys D: Appl. Phys. 32 (1999) 2151.
[7] P.V. Reddy, V.D. Reddy, J. Magn. Magn. Mater. 136 (1994) 279.
[8] G. Bonsdorf, K. Schaffer, H. Langbein, Eur. J. Solid State Org. Chem. 4 (1997) 1051.
[9] E. Wolska, K. Stempin, O. Krasnowska-Hobbs, Solid State Ionics 101–103 (1997) 527.
[10] M.N. Obrovac, O. Mao, J.R. Dahn, Solid State Ionics 112 (1998) 9.

[11] Y. Sakurai, H. Arai, J. Yamaki, Solid State Ionics 113 (1998) 29.
[12] P.P. Hankare, S.D. Jadhav, U.B. Sankpal, S.S. Chavan, K.J. Waghmare, B.K. Chougule, J. Alloys Compd. 475 (2009) 926.
[13] A. Beitollahi, M. Hoor, J. Mater. Sci. Mater. Electron. 14 (2003) 477.
[14] T.J. Trentler, K.M. Hickman, S.C. Geol, A.M. Viano, P.C. Gibbons, W.E. Bahro, Science 270 (1995) 1791.
[15] Y.P. Sui, X.F. Huang, Z.Y. Ma, W. Li, F. Qiao, K. Chen, K.J. Chen, J. Phys. Condens. Matter 15 (2003) 5793.
[16] Sonal Singhal, S.K. Barthwal, Kailash Chandra, Indian J. Pure Appl. Phys. 45 (2007) 821.
[17] E. Wolska, K. Stempin, O. Krasnowska-Hobbs, Sol. Stat. Ionics 101 (1997) 527.
[18] M.N. Obrovac, O. Mao, J.R. Dahn, Sol. Stat. Ionics 112 (1998) 9.
[19] Y. Sakurai, H. Arai, J. Yamaki, Sol. Stat. Ionics 113 (1998) 29.
[20] B.P. Ladgaonkar, C.B. Kolekar, A.S. Vaingankar, Bull. Mater. Sci. 25 (4) (2002) 351.
[21] R.D. Waldron, Phys. Rev. 99 (1955) 1727.
[22] Rajendran, R.C. Puller, A.K. Bhattacharya, D. Das, S.N. Chintalapudi, C.K. Majumdar, J. Magn. Magn. Mater, 232 (2001) 71.
[23] Wang, Y. Liu, Z. Zang, Handbook of Nanophase and Nanostuctured Materials (Vol. III: Materials Systems and Applications I), Kluwer Academic/Plenun Publishers, USA, 2003.
[24] Stoner, E.P. Wohlfarth, Phil. Trans. R. Soc. Lond. A Math. Phys. Sci. A 240 (1948) 599.
[25] S. Jan, Book of magnetic properties of materials, Intra-University Electron. Series 13 (1971) 89.